Acta Pharmaceutica Sinica B 2024;14(5):2194–2209

Chinese Pharmaceutical Association
Institute of Materia Medica, Chinese Academy of Medical Sciences

Acta Pharmaceutica Sinica B

www.elsevier.com/locate/apsb
www.sciencedirect.com

ORIGINAL ARTICLE

Branched glycopolymer prodrug-derived nanoassembly combined with a STING agonist activates an immuno-supportive status to boost anti-PD-L1 antibody therapy

Zhilin Li[a,d,†], Qianfeng Zhang[a,†], Zhiqian Li[a], Long Ren[a], Dayi Pan[a], Qiyong Gong[a,b,c], Zhongwei Gu[a], Hao Cai[a,*], Kui Luo[a,b,*]

[a]*Department of Radiology, Huaxi MR Research Center (HMRRC), Clinical Research Center for Breast, Department of Breast Surgery, Department of Thoracic Surgery and Institute of Thoracic Oncology, Frontiers Science Center for Disease-Related Molecular Network, State Key Laboratory of Biotherapy, West China Hospital Sichuan University, Chengdu 610041, China*
[b]*Functional and Molecular Imaging Key Laboratory of Sichuan Province, and Research Unit of Psychoradiology, Chinese Academy of Medical Sciences, Chengdu 610041, China*
[c]*Department of Radiology, West China Xiamen Hospital of Sichuan University, Xiamen 361021, China*
[d]*Key Laboratory of Medicinal Chemistry for Natural Resource, Ministry of Education, Yunnan Key Laboratory of Research and Development for Natural Products, School of Pharmacy, Yunnan University, Kunming 650500, China*

Received 27 November 2023; received in revised form 15 January 2024; accepted 20 January 2024

KEY WORDS

Glycopolymer;
Polymer prodrug;
Immunogenic cell death;
Nanoassembly;
Epirubicin;
STING pathway;
Immuno-supportive microenvironment;
Immunotherapy

Abstract Despite the great potential of anti-PD-L1 antibodies for immunotherapy, their low response rate due to an immunosuppressive tumor microenvironment has hampered their application. To address this issue, we constructed a cell membrane-coated nanosystem (mB4S) to reverse an immunosuppressive microenvironment to an immuno-supportive one for strengthening the anti-tumor effect. In this system, Epirubicin (EPI) as an immunogenic cell death (ICD) inducer was coupled to a branched glycopolymer *via* hydrazone bonds and diABZI as a stimulator of interferon genes (STING) agonist was encapsulated into mB4S. After internalization of mB4S, EPI was acidic-responsively released to induce ICD, which was characterized by an increased level of calreticulin (CRT) exposure and enhanced ATP secretion. Meanwhile, diABZI effectively activated the STING pathway. Treatment with mB4S in combination with an anti-PD-L1 antibody elicited potent immune responses by increasing the ratio of matured dendritic

*Corresponding authors.
E-mail addresses: chemcaihao@163.com (Hao Cai), luokui@scu.edu.cn (Kui Luo).
†These authors made equal contributions to this work.
Peer review under the responsibility of Chinese Pharmaceutical Association and Institute of Materia Medica, Chinese Academy of Medical Sciences.

https://doi.org/10.1016/j.apsb.2024.02.006

cells (DCs) and $CD8^+$ T cells, promoting cytokines secretion, up-regulating M1-like tumor-associated macrophages (TAMs) and down-regulating immunosuppressive myeloid-derived suppressor cells (MDSCs). Therefore, this nanosystem for co-delivery of an ICD inducer and a STING agonist achieved promotion of DCs maturation and $CD8^+$ T cells infiltration, creating an immuno-supportive microenvironment, thus potentiating the therapy effect of the anti-PD-L1 antibody in both 4T1 breast and CT26 colon tumor mice.

1. Introduction

Immune checkpoint inhibitor (ICI) therapies, such as anti-PD-L1 antibodies to block the PD-L1 axis, have been demonstrated to prevent tumor metastasis and recurrence[1,2]. However, the response rate of ICI in patients with triple-negative breast cancer (TNBC) is still low (less than 30%)[3,4]. Such a low response rate is predominantly due to an immunosuppressive microenvironment, leading to a low maturation ratio of dendritic cells (DCs) and a small fraction of infiltrated $CD8^+$ T cells into the tumor microenvironment[5–7]. Therefore, strategies to reverse the tumor immune microenvironment from immunosuppressive to immune-supportive are pursued in the tumor immunotherapy field[8–10].

When tumor cells are treated with anthracycline chemotherapeutics such as epirubicin (EPI), they can not only directly kill tumor cells, but also induce immunogenic cell death (ICD) to release tumor-associated antigens (TAAs) and damage-associated molecular patterns (DAMPs), both of which enhance the antigenicity and adjuvanticity to transform tumor cells from non-immunogenic to immunogenic[11,12]. Glycopolymers could be employed as a drug carrier for EPI to improve its delivery efficiency into tumor cells for efficiently inducing ICD and reducing its side effects. Novel glycopolymers with controllable chemical compositions, a topological structure, and a tunable molecular weight can be prepared by using active/controllable polymerization technologies and click chemistry, endowing them with great biodegradation, high drug loading, and controlled/stimuli-responsive release[13,14]. Previous studies have shown that branched polymers have better flexibility for multifunctional modifications and higher drug delivery capabilities due to their unique topological structures compared to their linear counterparts[15–18]. Our previous studies have shown that adjusting the hydrophilic and hydrophobic compositions in the branched polymers can enhance their self-assembly processes, thereby promoting the formation of stable nanostructures in an aqueous solution[19–21]. The branched polymers-derived nanostructures could be endowed with a homologous targeting ability after they are coated with tumor cell membranes to form biomimetic nanoparticles, thereby improving their homologous recognition by tumor cells[22,23].

Stimulator of interferon genes (STING), an innate immune pattern recognition receptor, is in the cytoplasmic endoplasmic reticulum, and it is known as a sensor of cytosolic DNA to invoke innate immunity[24,25]. The cytosolic DNA is detected by the cyclic GMP-AMP synthase and 2′−5′, 3′−5′ cyclic guanosine monophosphate-adenosine monophosphate (cGAMP) is produced, which can interact with the STING to phosphorylate and activate both TANK-binding kinase 1 (TBK1) and interferon regulatory factor (IFR-3)[26]. Activation of the STING pathway effectively stimulates DCs maturation, promotes tumor antigen cross-presentation, and enhances infiltration of $CD8^+$ T cells, therefore, this strategy has great potential in boosting the immunotherapeutic effect of anti-PD-L1 antibodies[27–29]. Activation of the STING pathway for cancer treatment has been achieved by the application of cyclic dinucleotides (CDNs) such as 2′, 3′-cGAMP or synthetic small molecules such as diABZI[30].

It is hypothesized that a STING agonist with the potential of promoting DCs maturation and $CD8^+$ T cells infiltration would synergize with EPI as an ICD inducer to create an immune-supportive microenvironment. Therefore, we constructed 4T1 cell membrane-coated glycopolymeric nanoparticles that were loaded with EPI and diABZI to potentiate the immunotherapeutic effect of an anti-PD-L1 antibody (Scheme 1). We prepared a 2-lactobionamidoethyl methacrylamide (LAEMA)-derived pH-sensitive branched poly(LAEMA) polymer, and modified its side chain through copper-free azide-alkyne click reaction to improve its assembly process and increase its drug loading capacity. The branched poly(LAEMA)-EPI prodrug self-assembled into stable nanoparticles and diABZI was efficiently encapsulated into the nanoparticles (termed as B4S). Furthermore, the 4T1 cell membrane was used to coat the polymeric nanoparticles to improve the homologous targeting efficiency. The 4T1 cell membrane-coated nanoparticles, termed as mB4S, had an improved cellular uptake efficiency by 4T1 cells. After uptake of mB4S, mB4S induced cell apoptosis, and calreticulin (CRT) exposure and ATP secretion were significantly enhanced in 4T1 cells, indicating that mB4S could effectively mediate ICD. Moreover, mB4S activated the STING pathway to facilitate DCs maturation and $CD8^+$ T cells infiltration, promote secretion of cytokines of IFN-γ, TNF-α, and IFN-β, down-regulate immunosuppressive immune cells including M2-like tumor-associated macrophages (TAMs) and myeloid-derived inhibitory cells suppressor cells (MDSCs), leading to an immune-responsive tumor microenvironment to enhance the therapeutic effect of the anti-PD-L1 antibody in 4T1-bearing and CT26-bearing mice.

2. Materials and methods

2.1. Materials

Epirubicin hydrochloride (EPI·HCl, HY-13624A) and CCK-8 kit (HY-K0301) were purchased from MCE Co., Ltd. (Shanghai, China), an ATP detection kit (S0027), a protease inhibitor cocktail

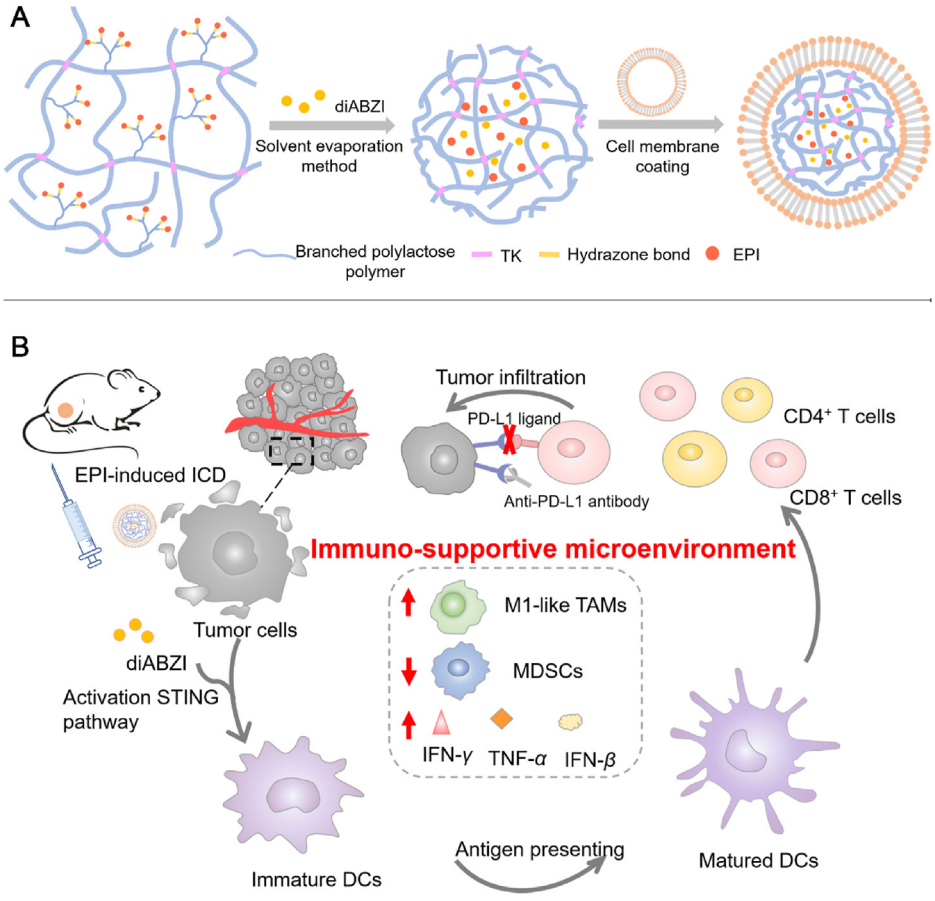

Scheme 1 Schematic illustration of construction of glycopolymeric nanoparticles which could be employed to induce ICD and activation of the STING pathway to potentiate the potency of anti-PD-L1 antibodies. (A) Construction of 4T1 cell membrane-coated branched glycopolymeric nanoparticles (mB4S) which accommodated EPI, an ICD inducer, and diABZI, a STING agonist. (B) The released EPI to induce ICD and diABZI to activate the STING pathway, up-regulating M1-like TAMs, down-regulating MDSCs and promoting cytokines secretion to remodel the immunosuppressive microenvironment to potentiate the therapeutic effect of anti-PD-L1 antibodies.

(100×) (P1006), a RAPI lysate buffer (P0013B), and a BCA protein assay kit (P0010) were obtained from Beyotime Biotechnology Co., Ltd. (Shanghai, China). Anti-mouse antibodies including BV605-Fixable viability stain (FVS) (Cat. No: 565694), BV510-CD45 (Cat. No: 563891), Alexa Fluor 700-CD3 (Cat. No: 557984), Percp-Cy5.5-CD8 (Cat. No: 551162), FITC-CD4 (Cat. No: 553046), Percp-Cy5.5-CD11b (Cat. No: 550993), FITC-Gr-1(Cat. No: 553126), BV421-F4/80 (Cat. No: 565411), Alexa Fluor 647-CD206 (Cat. No: 565250), APC-CD11c (Cat. No: 550261), Percp-Cy5.5-MHC II (Cat. No: 562363), and PE-Cy7-CD86 (Cat. No: 560582) were purchased from BD Bioscience Co., Ltd. (BD, New Jersey, USA). ELISA kits for IFN-γ (88-7314-88) and TNF-α (88-7324-88) analysis were purchased from Thermo Fisher Scientific Co., Ltd. (Thermo, Waltham, USA), and ELISA kit for IFN-β (luex-mifnbv2) analysis was purchased from Invivogen Co., Ltd. (Toulouse, Haute-Garonne, France). The STING agonist of diABZI (S8796) was purchased from Selleckchem Co., Ltd. (Houston, TX, USA). The anti-mouse-PD-L1 antibody (BE0101) was provided by Bio X Cell Co., Ltd. (Lebanon, PA, USA).

2.2. *Cell lines and animals*

4T1 murine breast cancer cells and CT26 murine colon cancer cells were obtained from Chinese Academy of Science Cell Bank (Shanghai, China). The cell culture was conducted in an incubator with 5% CO_2 at 37 °C. The PRMI 1640 medium (Hyclone, SH30809, Logan, UT, USA) containing 10% fetal bovine serum (FBS) (NEWZERUM, S010921, Christchurch, New Zealand) and 1% penicillin-streptomycin (Hyclone, SV30010, China) was used for 4T1 cells, while the DMEM-high glucose medium (Hyclone, SH30023, Logan, UT, USA) with 10% FBS (Gibco) and 1% penicillin−streptomycin (Hyclone) was used for CT26 cells. Female BALB/c mice of 6−8 weeks were purchased from Beijing Vitalstar Biotechnology Co., Ltd., and they were fed in a specified pathogen-free standard condition. All animal experiment procedures were approved by the Animal Ethics Committee of West China Hospital of Sichuan University (Animal Ethics Number: 2018148A and 2018150A).

2.3. *Synthesis of LAEMA-based branched polymeric prodrug*

LAEMA-based branched polymeric prodrugs were prepared by reversible addition-fragmentation chain transfer (RAFT) polymerization and copper-free azide-alkyne click reaction. The monomers, crosslinking agents, and chain transfer agents required for RAFT polymerization were prepared according to the synthesis routes in Supporting Information Scheme S1. Dibenzoazacyclooctyne

(DBCO)-modified compounds for click reactions were prepared according to the synthesis routes in Supporting Information Scheme S2. A branched polymer skeleton was prepared by RAFT polymerization. After modification of the side chains by clicking reaction, EPI, a chemotherapy drug, was covalently coupled into the polymers through pH-sensitive hydrazone bonds. Branched PLAEMA-$(EPI)_4$ was used as an example to illustrate the procedure (Supporting Information Scheme S3A). The other branched polymeric prodrugs (branched PLAEMA-$(EPI)_1$ and branched PLAEMA-$(EPI)_2$) were synthesized *via* a similar procedure (Scheme S3B).

2.3.1. Synthesis of branched poly(LAEMA-co-AzMA) as a branched polymer skeleton

LAEMA (1872.8 mg, 4 mmol), AzMA (134.5 mg, 0.8 mmol), MA-TK-MA (66.4 mg, 0.2 mmol), MA-TK-CTA (27.2 mg, 51.8 μmol) and the VA044 initiator (5.6 mg, 17.3 μmol) were dissolved in a solvent (H_2O/DMF = 2/7, *v*/*v*, 9.5 mL) and the mixture was bubbled with argon for 30 min. The reaction was carried out at 45 °C under a dark condition for 24 h and quenched in liquid nitrogen. The product was precipitated in acetone, isolated by centrifugation, and dialyzed (MWCO, 2 kDa) against deionized water. After freeze-drying, the final product (branched poly(LAEMA-*co*-AzMA)) was obtained (1.6 g, yield 77%).

2.3.2. Synthesis of branched PLAEMA-(NHNHBoc)$_4$ as a branched polymer intermediate

Branched poly(LAEMA-*co*-AzMA) (400 mg) and DBCO-$(NHNHBoc)_4$ (209 mg, 0.182 mmol) were dissolved in 50 mL of a solvent (H_2O/DMSO = 1/5, *v*/*v*). The solution was stirred at room temperature for 18 h in the dark. The resulting mixture was then dialyzed (MWCO, 8 kDa) against deionized water for 2 days and freeze-dried to obtain a crude product. The crude product was dissolved in a solvent (H_2O/DMF = 2/7, *v*/*v*, 3 mL). Branched PLAEMA-$(NHNHBoc)_4$ was isolated by precipitation into a mixture of acetone: diethyl ether (7/2, *v*/*v*, 50 mL), filtered and dried in a vacuum. Polymer intermediates including branched PLAEMA-$(NHNHBoc)_1$ and branched PLAEMA-$(NHNHBoc)_2$ were prepared according to the above method.

2.3.3. Synthesis of branched PLAEMA-(EPI)$_4$ as a branched polymeric prodrug

Branched PLAEMA-$(NHNHBoc)_4$ (400 mg) was dissolved in ultra-pure water (10 mL) in an ampule and the mixture was stirred under a nitrogen atmosphere. The ampule was heated for 6 h at 90 °C to realize the deprotection of hydrazide groups. Branched PLAEMA-$(NHNH_2)_4$ as a final product was obtained after lyophilization. The same protocol was used for the synthesis of branched PLAEMA-$(NHNH_2)_1$ and branched PLAEMA-$(NHNH_2)_2$.

Branched PLAEMA-$(NHNH_2)_4$ (300 mg) and EPI·HCl (285 mg) were dissolved in 20 mL of a NH_4OAc buffer (pH 5.7, 0.1 mol/L). The solution was then stirred in the dark at room temperature for 36 h. Subsequently, the solution was dialyzed (MWCO, 2 kDa) at 4 °C to completely remove excess free EPI. Finally, the solution was lyophilized to produce the final product, branched PLAEMA-$(EPI)_4$ (termed as B4). Branched PLAEMA-$(EPI)_1$ (termed as B1) and branched PLAEMA-$(EPI)_2$ (termed as B2) were prepared using a similar method as described above. The content of EPI in the prodrugs was determined by an UV−Vis spectrophotometer (Shimadzu Corporation, UV-1800, Tokyo, Japan).

2.4. In vitro drug release

The dialysis method was used to investigate the release characteristics of the prepared EPI-coupled polymers *in vitro*. 1.0 mL of the B1, B2, and B4 solution at a concentration of EPI 0.23 mg/mL was placed into a dialysis membrane (MWCO = 2 kDa), and it was dialyzed in 40 mL of PBS (pH 5.4 or pH 7.4) at an H_2O_2 concentration of either 0 or 10 mmol/L at 37 °C in a shaker (100 rpm). At predetermined time points, 1.5 mL of the release medium was withdrawn for sample analysis, while an equal volume of the fresh release medium was supplemented. The amount of EPI released at each time point was measured by a fluorescence spectrophotometer (Hitachi F-7000, Tokyo, Japan).

2.5. Cell cytotoxicity and cellular uptake

4T1 cells were seeded in 96-well plates and incubated with B1, B2, and B4 at different concentrations (0.39, 0.78, 1.56, 3.125, 6.25, 12.5, 15, 20, 25 μg/mL) for 48 h and PBS as a control. The culture medium was replaced with the RPMI 1640 culture medium containing the 10% CCK-8 and the incubation resumed for 2 h. The relative cell viability was calculated as shown in Eq. (1):

$$\text{Cell viability}\ (\%) = \left(OD_{\text{treated group}} - OD_{\text{blank group}}\right) \Big/ \left(OD_{\textit{control group}} - OD_{\text{blank group}}\right) \times 100 \quad (1)$$

where $OD_{\text{treated group}}$ is the absorbance value of cell treated with different concentration B1, B2 and B4, $OD_{\text{blank group}}$ is the absorbance value of cell untreated, $OD_{\text{control group}}$ is the absorbance value of culture medium with 10% CCK-8.

For evaluation of the uptake efficiency by 4T1 cells, they were seeded in 12-well plates and co-cultured with B1, B2, and B4 at the same EPI concentration of 1.5 μg/mL for 2, 4 and 8 h. After incubation, cells were collected and washed with PBS, then analyzed *via* a flow cytometer (Beckman, CytoFLEX, Suzhou, China).

2.6. Cell membrane-coated nanoparticles preparation and encapsulation of a STING agonist

4T1 cell membrane was collected *via* an ultracentrifuge (Beckman, Optima XPN-100, Brea, California, USA) as reported[31]. In brief, when the confluence of 4T1 cells reached nearly 80%−90%, they were washed with cold PBS three times. 4T1 cells were scraped and the cell solution was centrifuged (800×*g*, 5 min). The cell pellets were washed three times in a buffer solution supplemented with 30×10^{-3} mol/L Tris-HCl (pH = 7.0), 0.0759 mol/L sucrose, and 0.225 mol/L D-mannitol. A protease inhibitor cocktail was added into the cell suspension, and an ultrasonic probe (XiaoMei, XM-650T, KunShang, China) was used to mechanically disrupt the cells (Power = 35%, 3 s on and 3 s off, 3 min) in an ice bath. The homogenate was centrifuged (10,000×*g*, 30 min) to remove organelles, and the supernatant was centrifuged at 150,000×*g* for 60 min to obtain cell membrane. The collected cell membrane was resuspended in ultrapure water and stored at −80 °C.

To prepare cell membrane-coated nanoparticles, B4 loaded with a STING agonist was prepared by the solvent evaporation method. In brief, 1 mg of diABZI, a STING agonist, was dissolved in 1 mL of a mixture of methanol and acetone (1/1, *v*/*v*). Subsequently, the solution was dropwise added to 10 mL of the B4 solution at a concentration of 1.2 mg/mL. The mixture was stirred at room temperature for 24 h until organic solvents were

completely evaporated. A 2.2-micron filter membrane was used to remove the free agonist, and the self-assembled nanoparticles encapsulated with the agonist (named as B4S) were obtained. The Cy5-loaded B4S nanoparticles (named as $B4S^{Cy5}$) were prepared using the above-described method with minor modifications. 1.0 mg of diABZI and 0.13 mg of Cy5 carboxylic acid were added simultaneously to the B4 solution. The agonist and the near-infrared fluorescent dye were co-loaded into the hydrophobic core of the nanoparticles. The content of Cy5 in $B4S^{Cy5}$ was detected using a UV−Vis spectrophotometer (Shimadzu, Kyoto, Japan). The content of diABZI in the B4S was determined through high-performance liquid chromatography (HPLC, Shimadzu Corporation, Kyoto, Japan) with a UV−Vis detector at a wavelength of 325 nm. The mobile phase was acetonitrile (0.1% trifluoroacetic acid) and H_2O (0.1% trifluoroacetic acid). The drug loading (DL) of the STING agonist in B4S was calculated by the equation as shown in Eq. (2):

$$\mathrm{DL}\,(\%) = \left(W_{\text{loaded drug}} \,/\, W_{\text{nanoparticles}}\right) \times 100 \tag{2}$$

where $W_{\text{loaded drug}}$ is the weight of the loaded-drug in the nanoparticles, $W_{\text{nanoparticles}}$ is the total weight of the drug-loaded nanoparticles.

The collected cell membrane and B4S nanoparticles were mixed and the solution was then processed under an ultrasonic probe (Power = 50%, 3 s on and 3 s off, 30 times) in an ice bath. The cell membrane-coated nanoparticles were obtained and termed as mB4S. The size and zeta potential of mB4S were analyzed *via* a NanoBrook Series Size and Zeta Potential Analyzer (Brookhaven Instruments, NanoBrook Omni, NY, USA), and the morphology of mB4S was visualized under Transmission Electron Microscopy (TEM, FEI company, Tecnai G2 F20 S-TWIN, Hillsboro, OR, USA). The mB4S nanoparticles loaded with Cy5 (named as $mB4S^{Cy5}$) were prepared using the above-described method.

2.7. Flow cytometry analysis of apoptosis and cellular uptake

4T1 cells were seeded in 12-well plates at a density of 2×10^5 cells per well for 12 h. Subsequently, the culture medium containing EPI, B4, B4S, and mB4S (EPI concentration of 3 μg/mL) was added for 48 h co-culture. Cells were collected (300×*g*, 3 min) and resuspended in an Annexin V binding buffer solution and stained with Annexin V- Alexa Fluor 647 and DAPI according to the supplier's protocol for flow cytometry analysis (BD, FACS Celesta, New York, USA). For evaluation of the uptake efficiency in 4T1, RAW264.7, or 293T cells, the cells were seeded in 12-well plates and co-cultured with B4S or mB4S at the same EPI concentration of 1.5 μg/mL for 4 h. These cells were collected, washed with PBS, and analyzed *via* a flow cytometer (BD).

2.8. Western blots

4T1 cells were plated in 6-well plates and treated with EPI, diABZI, B4, B4S, and mB4S. A RAPI lysate buffer containing a phosphatase inhibitor and a protease inhibitor cocktail was added to the treated cells for cell lysis on ice. The lysate was centrifuged at 10,000×*g* for 30 min at 4 °C to obtain the supernatant. A BCA protein assay kit was used for protein quantification according to the manufacturer's instructions. A 1 × loading buffer was added into the collected supernatant and the mixture was boiled at 95 °C for 10 min. Electrophoresis using 10% SDS-PAGE gel was executed according to the standard protocol, and the proteins were transferred to a PVDF membrane. After blocking in a 5% BSA solution for 1 h, the band was incubated with primary antibodies on a shaker at 4 °C overnight and then with secondary antibodies for 1 h. A chemiluminescent solution was dropped on the band for visualization of the target protein *via* a chemiluminescence imaging system (BioRad, Hercules, CA, USA).

2.9. Inducing ICD in vitro

Immunofluorescent staining and an ATP assay kit were used to evaluate the ICD induced by mB4S. For observation of CRT exposure, 4T1 cells were plated in a confocal dish at a density of 3×10^4 cells per dish for 12 h and treated with EPI, B4, B4S, and mB4S for 12 h at the same EPI concentration of 3 μg/mL. The treated 4T1 cells were washed with PBS twice and fixed in 4% paraformaldehyde for 15 min. Cells were blocked in a 5% BSA solution for 2 h and incubated with an anti-CRT antibody diluted at 1:5000 overnight at 4 °C and an APC-conjugated secondary antibody for 2 h. The cell nuclei were stained with DAPI for 8 min and washed gently twice with PBS for visualization *via* a confocal scanning laser microscope (CLSM, Nikon, AIRMP$^+$, Tokyo, Japan, λ_{ex} = 633 nm, λ_{em} = 660 nm). To detect the ATP concentration in the cell culture supernatant, 4T1 cells were seeded in 6-well plates (5×10^5 cells per well) and co-cultured with EPI, B4, B4S, and mB4S for 12 h. The supernatant was collected and centrifuged (800×*g*, 3 min) to remove cell debris, and the ATP content was detected according to the manufacturer's instructions.

2.10. In vivo biodistribution study

4T1-bearing mice were randomly divided into three groups for evaluation of *in vivo* biodistribution of free Cy5, $B4S^{Cy5}$, and $mB4S^{Cy5}$ (n = 3). The mice were intravenously injected with the three formulations at the same Cy5 dose of 1.5 mg/kg. At the predetermined time points of 1, 2, 4, 8, 12, and 24 h, the mice were anesthetized for *in vivo* imaging *via* an IVIS spectrum system (PerkinElmer, Waltham, MA, USA). These tumor-bearing mice were sacrificed at 24 h after injection and major organs (heart, lung, spleen, liver, and kidney) and tumors were harvested for *ex vivo* imaging at 640 nm excitation and 680 nm emission.

2.11. Anti-tumor therapy in vivo

To establish a subcutaneous 4T1-bearing mice model, 1×10^6 of 4T1 cells in 60 μL PBS were subcutaneously injected into the right back of the mice. The length and width of the tumor were monitored and the tumor volume was calculated from Eq. (3):

$$\text{Tumor volume} = 0.5 \times L \times W^2 \tag{3}$$

where the L and W are the length and width of tumors, respectively.

When the tumor volume reached 75−100 mm^3, mice were randomly divided into eight groups (n = 5): saline, EPI, a STING agonist (diABZI), B4, B4S, mB4S, anti-PD-L1 antibody, and mB4S + anti-PD-L1 antibody for anti-tumor therapy. The mice were intravenously injected three times with the above formulations every 3 day at the same dose of EPI 8 mg/kg and diABZI 1.5 mg/kg. An anti-PD-L1 antibody was intraperitoneally injected at a dose of 100 μg on the following day. During the treatment period, the tumor volume and body weight were monitored every other day. At the end of the treatment, major organs and tumors

were collected for H&E and TUNEL staining analysis. To further explore the anti-tumor effect of mB4S, a subcutaneous CT26-bearing mice model was established. The treatment scheme was the same as that for the subcutaneous 4T1-bearing mice model while CT26 cell membrane was used for cell membrane coating.

2.12. *Activation of immune responses in 4T1-bearing mice*

To analyze the infiltrated immune cells in the tumor microenvironment, the mice with the subcutaneous breast cancer model were intravenously injected with saline, EPI, a STING agonist (diABZI), B4, B4S, mB4S, anti-PD-L1 antibody, and mB4S + anti-PD-L1 antibody at the same treatment dose of EPI, diABZI and the antibody as that for the *in vivo* anti-tumor therapy. The mice were euthanized on next day to harvest tumors and spleens to prepare cell suspensions. Briefly, tumors were cut into pieces in cold PBS and centrifuged to collect the tumor tissue supernatant for ELISA analysis of cytokines including IFN-γ, TNF-α, and IFN-β. A digestive solution containing hyaluronidase/collagenase IV and deoxyribonuclease I was added into the tumor pellets, and the mixture was shaken at a speed of 120 rpm at 37 °C for 30 min on a shaker. The cell suspensions were filtered through a 70 μm cell strainer. 1×10^7 cells were stained with BV605-FVS at 4 °C for 30 min and blocked with 1 μL of the Fc antibody in 100 μL of a staining buffer for 30 min at 4 °C. The cells were then stained with BV510-CD45, Alexa Fluor 700-CD3, FITC-CD4, and PerCp-Cy5.5-CD8 anti-mouse monoclonal antibodies to evaluate the ratio of $CD8^+$ T cells ($CD3^+CD8^+$), or APC-Cy7-CD45, APC-CD11c, Percp-Cy5.5-MHC II, PE-Cy7-CD86 to count the matured DCs ($CD11c^+$MHC II $^+CD86^+$). To analyze the percentage of M1-like TAMs ($CD11b^+$ $F4/80^+CD86^+$) and MDSCs ($CD11b^+Gr\text{-}1^+$), cells were stained with BV510-CD45, Percp-Cy5.5-CD11b, FITC-Gr-1, BV421-F4/80, PE-Cy7-CD86, and Alexa Fluor 647-CD206. To prepare the spleen cell suspensions, the spleen was ground on ice and passed through a 70 μm cell strainer. 5 mL of an erythrocyte lysis solution was added to remove erythrocytes. The lysate was centrifuged (800×*g*, 3 min) and washed to obtain spleen cells. The spleen cells were stained in a similar procedure as that for tumor cells to evaluate the ratio of $CD8^+$ T cells ($CD3^+CD8^+$) and matured DCs ($CD11c^+$MHC II $^+CD86^+$).

2.13. *Statistical analysis*

GraphPad Prism 6 software was used for data analysis. All quantitative values are presented as mean ± SD. Student's *t*-test was used for statistical analysis of differences between two groups, and the results were considered significant when $^*P < 0.05$, $^{**}P < 0.01$, $^{***}P < 0.001$, and $^{****}P < 0.0001$.

3. Results and discussion

3.1. *Synthesis of EPI-coupled branched glycopolymer prodrugs*

In this study, we designed and synthesized branched polymeric prodrugs with different structures *via* RAFT polymerization and copper-free azide-alkyne click reaction, and their potential as a polymeric nano-drug delivery system was evaluated. First, the monomers of AzMA, LAEMA, and MA-TK-MA as a crosslinking agent and MA-TK-CTA as a chain transfer agent were synthesized for the synthesis of branched polymers (Supporting Information Scheme S1). Subsequently, small molecular compounds of DBCO-$(NHNHBoc)_1$, DBCO-$(NHNHBoc)_2$, and DBCO-$(NHNHBoc)_4$ containing acyl hydrazine bond groups were synthesized for click reactions (Supporting Information Scheme S2). The structures of all synthesized compounds were characterized and their purity was confirmed by ^{1}H NMR, ^{13}C NMR, and liquid chromatography-mass spectrometry (LC-MS) (Supporting Information Figs. S1−S18). Based on the successful synthesis of various compounds, poly(LAEMA-*co*-AzMA) with a branched structure was prepared through a "one pot" method *via* RAFT polymerization (Supporting Information Scheme S3). As shown in Supporting Information Fig. S19A, in the ^{1}H NMR spectrum of poly(LAEMA-*co*-AzMA), characteristic peaks of the glycopolymer (4.60 ppm, 4.55 ppm, 4.40 ppm) and CTA (7.94 ppm, 7.70 ppm, 7.53 ppm) were observed. No characteristic peak of the double bond in the monomers appeared in the spectrum, indicating that the unreacted monomer was completely removed from poly(LAEMA-*co*-AzMA). In addition, the GPC results showed that poly(LAEMA-*co*-AzMA) had a number-average (M_n) molecular weight of 27.7 kg/mol and dispersity ($Đ$) of 1.23, indicating that the high-molecular-weight branched polymeric skeleton was successfully prepared (Fig. S19B). It was noteworthy that a distinct characteristic peak of the azide group was observed at 2100 cm^{-1} in the infrared spectrum of poly(LAEMA-*co*-AzMA) (Supporting Information Fig. S20), suggesting that the azide group was successfully introduced into the polymer skeleton.

We coupled DBCO-$(NHNHBoc)_1$, DBCO-$(NHNHBoc)_2$, and DBCO-$(NHNHBoc)_4$ with branched poly (LAEMA-*co*-AzMA) to obtain three polymer intermediates with different side chain structures. Due to a similar composition of the obtained polymers, the characterization results were analyzed using branched PLAEMA-$(NHNHBoc)_4$ as an example. As shown in Supporting Information Fig. S21, a distinct characteristic peak of the Boc group was observed at 1.4 ppm in the ^{1}H NMR spectrum of branched PLAEMA-$(NHNHBoc)_4$ when compared to that of branched poly(LAEMA-*co*-AzMA), indicating successful coupling of DBCO-$(NHNHBoc)_4$ to the polymer side chain.

Subsequently, branched PLAEMA-$(NHNHBoc)_4$ was deprotected under a heating condition to expose the acyl hydrazine bonds, which could form pH-sensitive hydrazone bonds by reacting with the ketone carbonyl group of EPI[32]. As shown in Fig. S22, the Boc characteristic peak disappeared in branched PLAEMA-$(NHNH_2)_4$, indicating the successful removal of the Boc groups. As shown in Supporting Information Fig. S23, the EPI characteristic spectrum was observed in the UV−Vis spectra of B4, branched PLAEMA-$(EPI)_4$, compared to PLAEMA-$(NHNH_2)_4$, a drug-free polymer, suggesting that EPI was successfully linked to the polymer. Since the ^{1}H NMR spectrum of B4 (Supporting Information Fig. S24) did not display a distinct characteristic peak of EPI, the prodrug may form a self-assembled structure in an aqueous solution. Similarly, branched polymer prodrugs with different side chains including B1, branched PLAEMA-$(EPI)_1$, and B2, branched PLAEMA-$(EPI)_2$, were synthesized. The characterizations of B1 were shown in Supporting Information Figs. S25−S27 and Supporting Information Figs. S28−S30 for B2.

As shown in Fig. 1A, the branched polymeric prodrug structure contained hydrophilic glycopolymers and hydrophobic EPI drugs, so it may undergo self-assembly under $\pi-\pi$ stacking and hydrophilic hydrophobic interactions. Supporting Information Table S1 showed that the synthetic prodrugs of B1, B2, and B4 self-assembled into nanoparticles in an aqueous solution and their

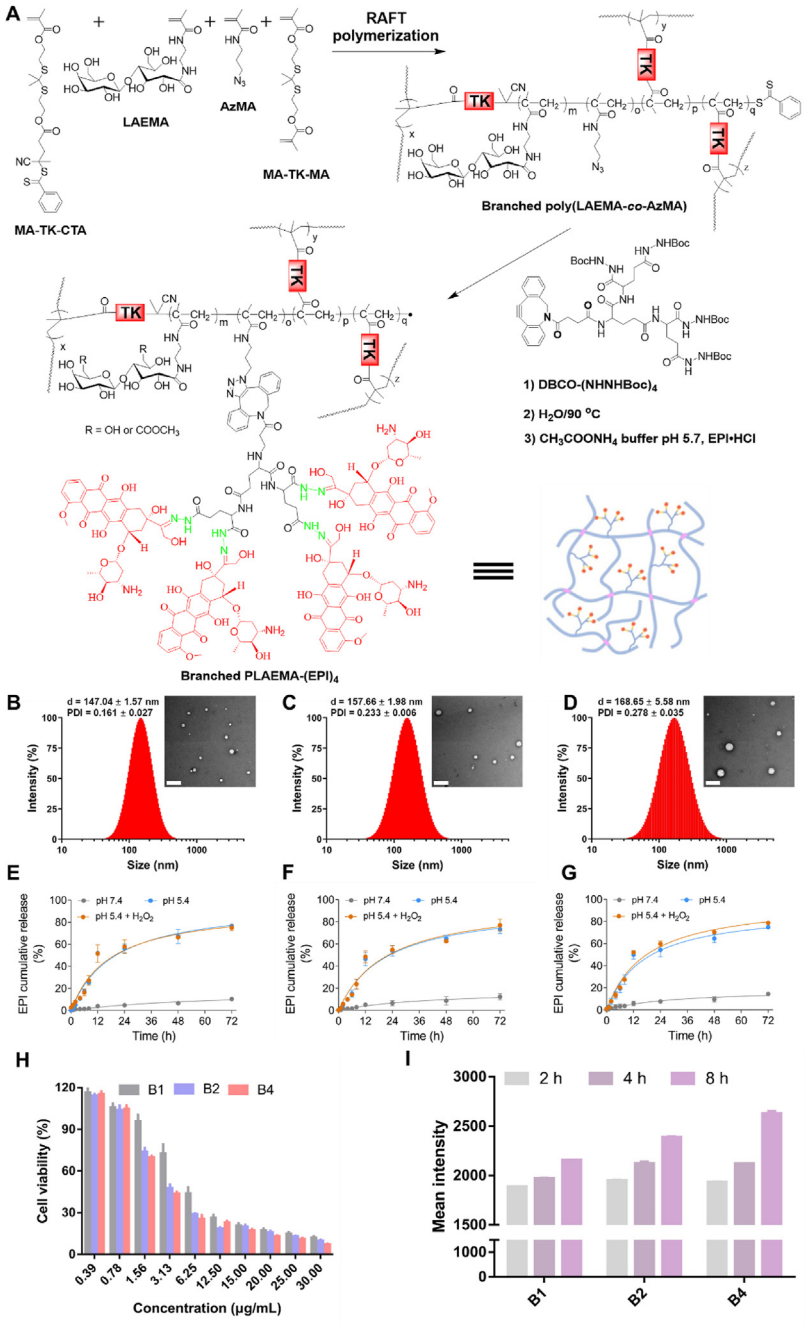

Figure 1 Characterizations of branched glycopolymer prodrugs of B1, B2, and B4. (A) The synthesis route and structural diagram of branched PLAEMA-$(EPI)_4$ (termed as B4). (B−D) The sizes and TEM images of B1, B2, and B4 (scale bar = 500 nm). (E−G) EPI release curves of B1, B2, and B4 in pH 7.4 PBS, pH 5.4 PBS, and pH5.4 PBS containing H_2O_2 (10 mmol/L). (H) Cytotoxicity of B1, B2, and B4 at different concentrations against 4T1 cells *via* the CCK-8 kit (Data are presented as mean ± SD, $n = 5$). (I) The efficiency of endocytosing B1, B2, and B4 by 4T1 cells after co-culture for 2, 4, and 8 h (Data are presented as mean ± SD, $n = 3$).

particles sizes were 147.04 ± 1.57, 157.66 ± 1.98, and 168.65 ± 5.58 nm, respectively. The surface charges of B1, B2, and B4 nanoparticles were electrically neutral. In addition, the EPI drug loading in B1, B2, and B4 was determined by the ultraviolet absorption method, and it was 8.5%, 16.3%, and 23.4%, respectively. As the content of hydrazide bonds in the polymer side chains increased, the drug loading in the polymers showed an increased trend, indicating that side chain modification of the branched glycopolymers could effectively regulate their drug loading capacity. It could be seen from the TEM images in Fig. 1B−D that these prodrug nanoparticles were spherical, and their size was around 150 nm. In the presence of acid-sensitive hydrazone bonds in the branched polymers, a small fraction of EPI (less than 15%) was released from three branched polymer prodrugs within 72 h at pH 7.4, while up to 80% EPI was released at pH 5.4 within the same time frame (Fig. 1E−G), indicating that the prepared prodrug nanoparticles could acid-responsively release the incorporated drug.

3.2. Cytotoxicity and cellular uptake of EPI-coupled branched-PLAEMA prodrug nanoparticles

Cell cytotoxicity of B1, B2, and B4 was evaluated against 4T1 cells *via* a CCK-8 kit, and their IC_{50} values were calculated. As presented in Fig. 1H, the cell cytotoxicity of B4 was stronger than that of B1 and B2 under the same concentration, and the IC_{50} values were 4.20, 1.82, and 1.63 μg/mL for B1, B2, and B4, respectively (Supporting Information Fig. S31). The 4T1 cell uptake efficiency for three branched polymer prodrugs was analyzed *via* flow cytometry. As shown in Fig. 1I—B1, B2, and B4 nanoparticles were uptaken by 4T1 cells in a time-dependent manner. It was pronounced that 4T1 cells showed a higher level of cellular uptake of B4 nanoparticles, and the mean fluorescence intensity in B4-containing 4T1 cells was 1.15- and 1.27-fold of that of B1 or B2-containing 4T1 cells after they were co-cultured for 8 h. Furthermore, the CLSM images verified that 4T1 cells efficiently internalized B4 nanoparticles (Supporting Information Fig. S32). Since B4 nanoparticles had a relatively high uptake efficiency by 4T1 cells, the cytotoxicity of B4 nanoparticles was slightly stronger than that of B1 and B2 nanoparticles.

3.3. Construction and characterizations of mB4S

Since B4 nanoparticles outperformed B1 and B2 nanoparticles in the drug loading efficiency, cytotoxicity, and the cellular uptake efficiency, B4 nanoparticles were selected for the following studies. The solvent evaporation method was used to encapsulate diABZI, a STING agonist, into B4 nanoparticles, and the prepared product was termed as B4S. The drug loading efficiency of diABZI into B4S was 5.6%, indicating that branched polymer could effectively load the agonist.

It is reported that tumor cell membrane-coated nanoparticles endow them with the property of homologous targeting[33]. To improve the targeted delivery of B4S, the 4T1 cell membrane was collected and coated as an outer shell of B4S nanoparticles (termed as mB4S). From the TEM images (Fig. 2A and B), there was a layer of cell membranes on the periphery of B4S nanoparticles, and the thickness of the cell membrane was estimated to be around 15 nm. The zeta potential of B4S and mB4S nanoparticles was 0.14 ± 0.41 and -24.86 ± 0.99 mV, respectively (Fig. 2C). The potential change from a neutral to negative charge after coating with cell membranes indicated effective coating of cell membranes onto B4S.

The stability of mB4S in distilled water, PBS, PBS +10% FBS was assessed *via* dynamic light scattering (DLS). As shown in Supporting Information Fig. S33, the size and PDI of mB4S nanoparticles had a negligible change during 72 h, indicating a stable structure of mB4S. The dialysis method was used to investigate the release profiles of diABZI and EPI from B4S and mB4S *in vitro*. As shown in Supporting Information Fig. S34, mB4S exhibits a pronounced pH-responsive capability for releasing diABZI and EPI. Under pH 5.4 conditions, over 70% of diABZI is released from mB4S within 24 h. Additionally, the cumulative release rate of EPI at pH 5.4 within 72 h significantly exceeds that at pH 7.4.

3.4. Cellular uptake efficiency of mB4S

Flow cytometry (Beckmann) and CLSM (Nikon) were used to evaluate the cell uptake efficiency of mB4S in homologous 4T1 cells and heterologous RAW264.7 and 293T cells. From the flow cytometry quantitative analysis results (Fig. 2D), the mean fluorescence intensity in 4T1 cells after co-incubation with mB4S was 1.21-fold higher than that in the B4S-treated group. Correspondingly, the red fluorescence of mB4S in 4T1 cells shown in the CLSM images (Fig. 2F) was stronger than that of B4S, and the fluorescence intensity in the mB4S-treated cells was 1.25-fold higher than that in the B4S group (Supporting Information Fig. S35). The above results suggested that the cell membrane coating could improve the cellular uptake efficiency of B4S by 4T1 cells. Meanwhile, the uptake efficiency of mB4S by heterologous cells including RAW264.7 and 293T cells was lower than that of B4S nanoparticles (Fig. 2E). These cellular uptake results suggested that coating of 4T1 cell membrane onto B4S nanoparticles could promote their internalization by 4T1 cells due to the presence of specific proteins on the cell membrane surfaces but hamper their cellular uptake by heterologous cells.

3.5. Apoptosis and activation of the STING pathway

4T1 cell apoptosis after treatment with EPI, B4, B4S, and mB4S was evaluated by an Annexin V- Alexa Fluor 647 apoptosis kit *via* a flow cytometer. As shown in Fig. 3A and B, the apoptotic rate of cells treated with mB4S was 48.8%, while it was 40.5% in the B4S-treated group, which indicated that mB4S may be able to effectively induce 4T1 cells apoptosis. diABZI as a STING agonist could activate the STING pathway to mediate innate immune responses, and it has been demonstrated to have a potent immune adjuvant effect[34]. 4T1 cells were treated with diABZI, B4, B4S, and mB4S for 36 h and proteins were collected to confirm the activation of the STING pathway by these formulations. Stimulation of the STING pathway often leads to upregulation of TBK1 and activation of IRF-3[28]. The Western blot images in Fig. 3C and their quantitative results in Supporting Information Fig. S36 for the expression levels of p-TBK1 and p-IFR-3 confirmed that p-TBK1 and p-IFR-3 were up-regulated in the mB4S-treated group compared to the control group, suggested that the STING pathway was activated in the 4T1 cells after exposure to mB4S.

3.6. In vitro ICD induced in 4T1 cells

ICD could be induced in tumor cells treated with chemotherapeutics such as EPI to promote CRT exposure and ATP secretion, which help transform non-immunogenic tumor cells to immunogenic cells[35]. As shown in Fig. 3D and Supporting Information Fig. S37, 4T1 cells treated with EPI resulted in a low level of CRT exposure, while a distinct red fluorescence signal was observed in the B4S or mB4S-treated group, suggesting that B4S or mB4S intervention could induce a remarkable level of CRT exposure. The ATP concentration in the supernatant was detected *via* an ATP assay kit according to the manufacturer's instructions after the 4T1 cells were co-cultured with EPI, B4, B4S, and mB4S. The ATP concentration in the mB4S-treated group was 2.15 times that in the EPI-treated group, while negligible changes were seen in the ATP concentration after cells were exposed to B4S and mB4S (Fig. 3E). Therefore, mB4S exposure could mediate CRT exposure and promote ATP secretion, suggesting its effectiveness in inducing ICD in the 4T1 cells.

3.7. In vivo biodistribution and anti-tumor therapeutic effect

The tumor-targeting ability of nanoparticles plays a critical role in tumor therapy[36]. It has been reported that a tumor cell membrane coating of nanoparticles could promote their tumor site

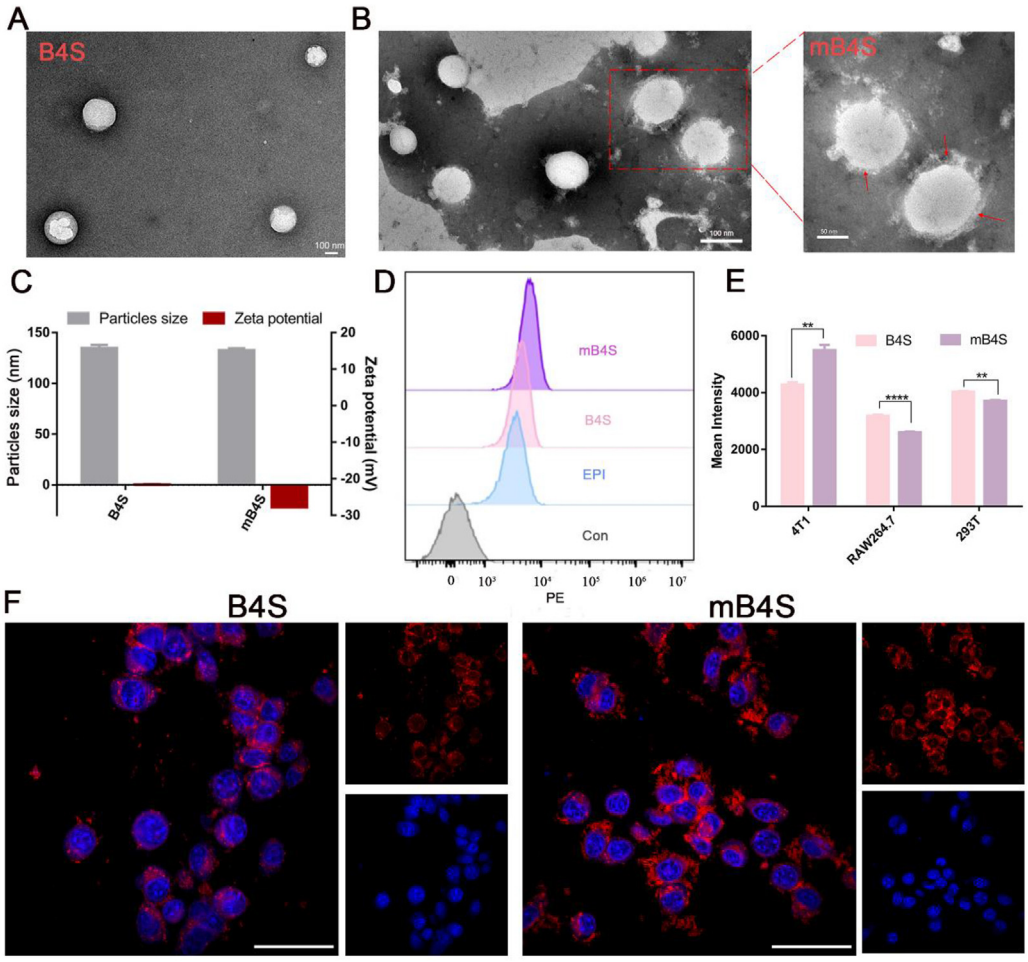

Figure 2 Preparation and cell uptake efficiency of cell membrane-coated nanoparticles. (A, B) TEM images of B4S and mB4S. (C) Changes in the particle size and zeta potential before and after cell membrane coating. (D) Uptake efficiencies of B4S and mB4S by 4T1 cells. (E) The mean fluorescence intensity of B4S and mB4S in 4T1, 293T, and RAW264.7 cells (Data are presented as mean ± SD, $n = 3$, $^{**}P < 0.01$, $^{****}P < 0.0001$ *vs.* B4S group). (F) Representative CLSM images of 4T1 cells co-cultured with B4S and mB4S for 3 h. Blue for the cell nucleus and red for EPI (scale bar = 50 μm).

accumulation[37]. In this study, 4T1-bearing mice were intravenously injected with free Cy5, B4S^{Cy5}, and mB4S^{Cy5} at the same Cy5 dose of 1.5 mg/kg for evaluation of their *in vivo* biodistribution. After intravenous injection of free Cy5, B4S^{Cy5}, mB4S^{Cy5} into 4T1-bearing mice, the Cy5 fluorescence intensity at the tumor site in the mB4S^{Cy5} group was stronger than that in the free Cy5 and B4S^{Cy5} groups at 24 h post-administration (Supporting Information Fig. S38A and S38C), indicating that mB4S^{Cy5} nanoparticles could accumulate at the tumor site through tumor cell membrane coating-mediated homologous targeting, while free Cy5 could be rapidly cleared. The *ex vivo* images (Fig. S38B and S38D) of main organs and tumors at 24 h post-injection also confirmed that the strongest fluorescence intensity was observed in the tumors of the mB4S^{Cy5} group, indicating that mB4S^{Cy5} nanoparticles could efficiently target tumors. Moreover, pharmacokinetic analysis results were shown in Supporting Information Fig. S39, the EPI concentration in the mB4S group was reduced slowly when compared with the B4S and free EPI group. The half-time of mB4S nanoparticles was pronouncedly prolonged to 7.71 h, while it was 4.49 h for B4S (Supporting Information Table S2), indicating that the cell membrane coating could increase the circulation time of cell membrane-coated nanoparticles.

Subcutaneous 4T1 breast cancer and CT26 colorectal cancer models were established to assess the *in vivo* anti-tumor therapeutic effect of mB4S. The treatment schedule scheme was shown in Fig. 4A. According to the tumor volume curve (Fig. 4B), a continuous growth trend in the tumor volume was seen after injections of EPI and the anti-PD-L1 antibody, while interventions with B4S and mB4S effectively inhibited the tumor growth. The most effective inhibition of tumor growth was found in the group treated with mB4S in combination with the anti-PD-L1 antibody. In addition, the average tumor weight in the group treated with mB4S in combination with the anti-PD-L1 antibody was 207 mg, which was around 1/5 of that in the free EPI-treated group (1143 mg) and 1/9 of that in the anti-PD-L1 antibody-treated group (1863 mg) (Fig. 4D). In this context, EPI-coupled polymeric nanoparticles induced ICD and the STING agonist activated the STING pathway, leading to a significant enhancement in the treatment effect of the anti-PD-L1 antibody. The body weight change curves during the therapy period (Fig. 4C) revealed that treatment with the STING agonist and EPI led to a loss in the body

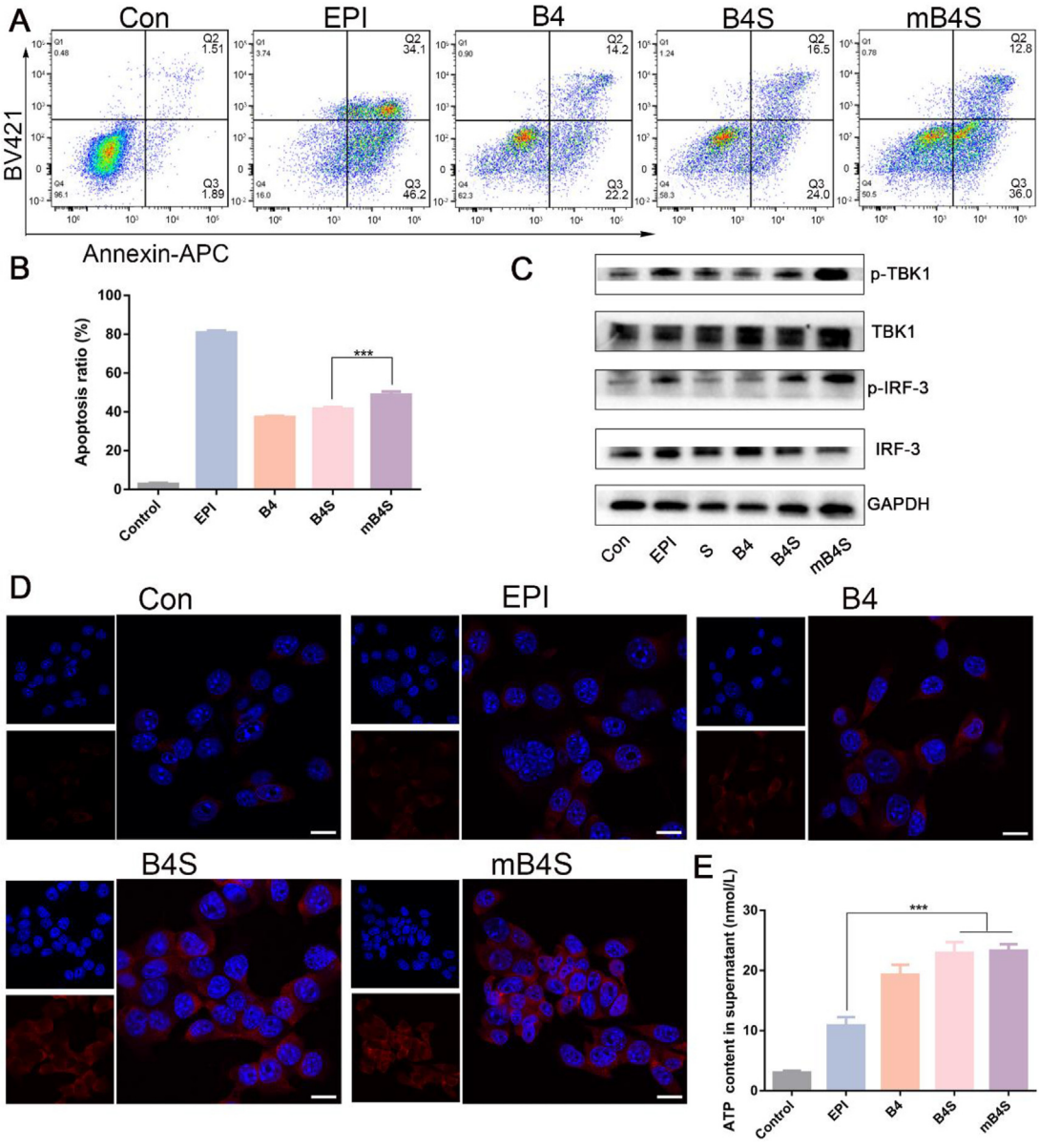

Figure 3 *In vitro* anti-tumor effect of mB4S on 4T1 cells. (A) Apoptosis analysis of 4T1 cells after treatment with EPI, B4, B4S, and mB4S *via* flow cytometry. (B) Quantification of the apoptosis rate after different treatments. (C) Western blot analysis of p-TBK1, TBK1, p-IRF-3, and IRF-3 after treatment with EPI, diABZI (S), B4, B4S, and mB4S. (D) Representative CLSM images of CRT exposure in 4T1 cells after co-culture of them with EPI, diABZI, B4, mB4S, and mB4S nanoparticles (Blue: cell nucleus; Red: CRT; Scale bar = 50 μm). (E) The ATP content in the supernatant after treatment with PBS, EPI, B4, B4S, and mB4S (Data are presented as mean ± SD, $n = 3$, $^{***}P < 0.001$ *vs.* EPI treated group).

weight after the first treatment, while there was a negligible change in the body weight in the mice treated with mB4S, or mB4S in combination with the antibody. This indicated that the nano-drug delivery system can effectively reduce the toxicity of small molecule therapeutic agents, consistent with previous reports[38,39]. Furthermore, the main organs including the heart, liver, spleen, and kidney did not show obvious pathologic changes (Supporting Information Fig. S40), suggesting this nano-drug delivery system has no pronounced side effects. Serum biochemistry analysis was conducted to evaluate liver and kidney toxicity of mB4S. From Supporting Information Fig. S41, the levels of alanine aminotransferase (ALT), aspartate aminotransferase (AST), alkaline phosphatase (ALP), creatinine (CREA), and urea (UREA) remained normal in the mB4S treated group compared to the saline-treated group, while both free EPI and diABZI induced a certain degree of liver and renal injury. Moreover, the H&E-stained lung slices revealed that the therapy of combining mB4S and the anti-PD-L1 antibody effectively prevented pulmonary metastasis compared with the monotherapy with EPI or the anti-PD-L1 antibody (Supporting Information Fig. S42). The predominant red fluorescence signal was seen in the TUNEL staining images (Fig. 4E and Supporting Information Fig. S43) of the tumor tissue treated with mB4S in combination with the anti-PD-L1 antibody, suggesting that the combined therapy could potently induce apoptosis of 4T1 cells. These results supported that mB4S combined with the anti-PD-L1 antibody

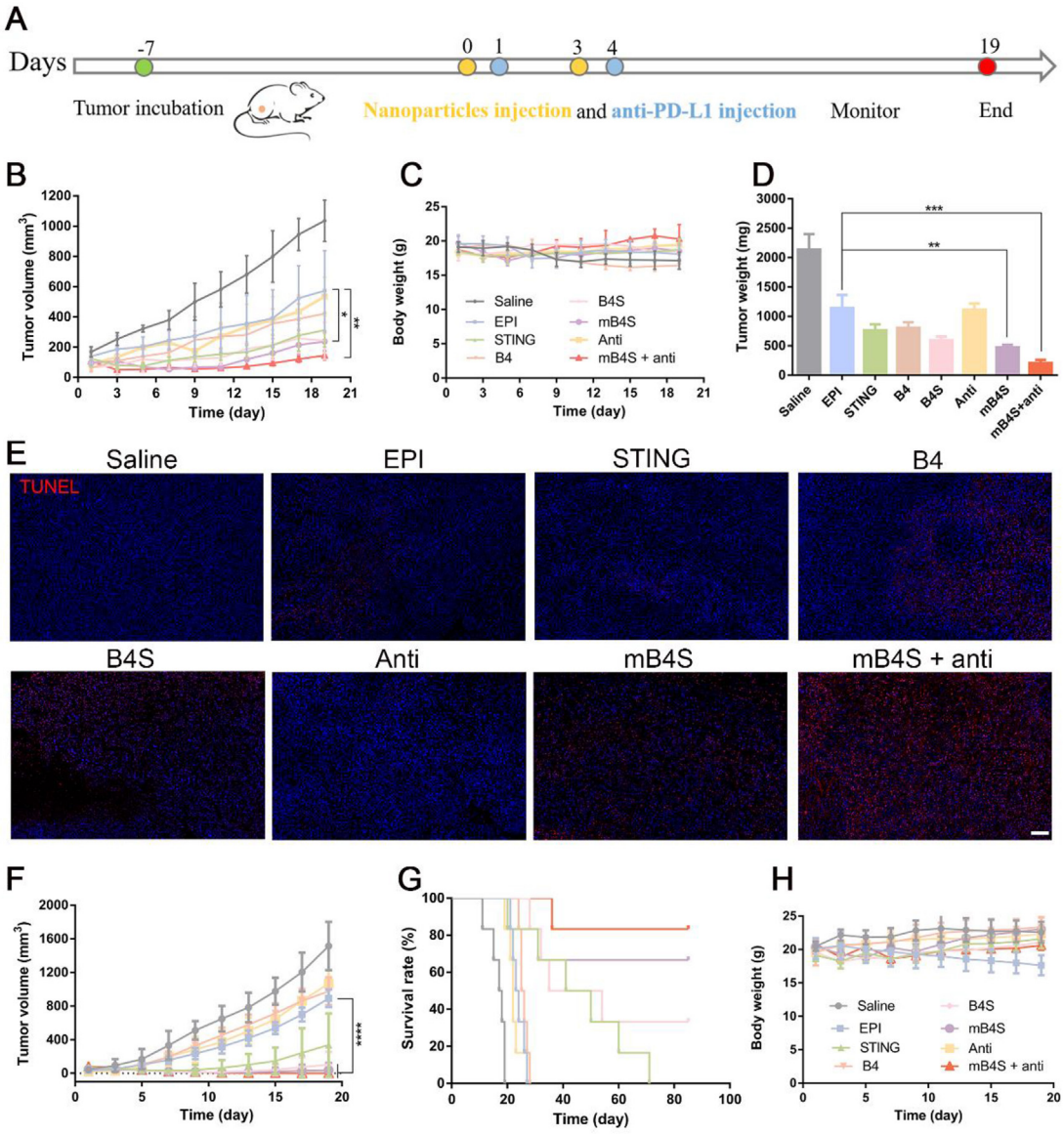

Figure 4 *In vivo* anti-tumor effect of mB4S combined with an anti-PD-L1 antibody in the 4T1-bearing and CT26-bearing mice. (A) Schematic diagram of the treatment schedule. (B) Tumor volume, (C) body weight, and (D) tumor weight in the 4T1-bearing mice after treatment with saline, EPI, diABZI, B4, B4S, mB4S, anti-PD-L1 antibody, and mB4S + anti-PD-L1 antibody (Data are presented as mean ± SD, $n = 5$, $^{*}P < 0.05$, $^{**}P < 0.01$, $^{***}P < 0.001$ *vs*. EPI-treated group). The dose of EPI was 8 mg/kg, 1.5 mg/kg for diABZI, and 100 μg for the anti-PD-L1 antibody; (E) TUNEL staining of tumor tissues at the end of treatment (Blue: cell nucleus; Red: TUNEL; Scale bar = 100 μm). (F) Tumor volume, (G) survival curve and (H) body weight in the CT26-bearing mice after the same treatment as that in the 4T1-bearing mice (Data are presented as mean ± SD, $n = 6$, $^{****}P < 0.0001$ *vs*. EPI-treated group).

displayed the most potent anti-tumor therapeutic effect in the 4T1 breast cancer model among eight treatment groups.

Furthermore, the anti-tumor effect was investigated in the CT26-bearing colon cancer mice. As shown in Fig. 4F, the treatment with EPI, diABZI, B4, B4S, the anti-PD-L1 antibody, and mB4S led to different levels of delaying the tumor progression. Treatment with a single therapeutic drug including EPI and the anti-PD-L1 antibody resulted in slight inhibition of tumor growth, while significant inhibition of tumor growth at the end of the therapy period was seen in the groups treated with B4S and mB4S. The therapy with mB4S in combination with the anti-PD-L1 antibody effectively eliminated 83.3% of CT26 tumors, and the inhibition rate was significantly higher than that in the group treated with EPI and the anti-PD-L1 antibody, suggesting that the synergistic effect of EPI-induced ICD and activation of the STING pathway resulted in an enhancement in the therapeutic efficacy of EPI and diABZI. Moreover, the survival curve (Fig. 4G) displayed that the combined treatment with mB4S plus the anti-PD-L1 antibody could significantly prolong the survival rate of the CT26-bearing mice, which indicated a great potency of mB4S in combination with the anti-PD-L1 antibody for their anti-tumor therapy. The body weight of the mice treated with B4S, mB4S, the combined mB4S and the antibody barely changed during the treatment period, while it was distinctively reduced in

the EPI-treated group (Fig. 4H), indicating that the combined therapeutic formulation of mB4S and the antibody did not exhibit significant toxicity in the CT26-bearing mice.

3.8. *In vivo activation of immune responses*

The immune activation in the tumor-bearing mice was evaluated after treatment with saline, EPI, diABZI, B4, B4S, mB4S, anti-PD-L1 antibody, and mB4S + anti-PD-L1 antibody. Activated immune cells such as matured DCs and infiltrated $CD8^+$ T cells in the tumor microenvironment are key indicators for effective anti-tumor immunotherapy[40]. mB4S-induced ICD and released TAAs and DAMPs could promote DCs to present antigens to T cells for invoking the cancer-immunity cycle[41]. It can be seen from Supporting Information Fig. S44 that the treatment of mB4S combined with the anti-PD-L1 antibody induced potent CRT exposure, which indicated that the combined treatment effectively mediated ICD in tumor tissues. As shown in Fig. 5A and B, the ratio of matured DCs ($CD11c^+MHC\ II\ ^+CD86^+$) in tumor tissue with a gating strategy exhibited in Supporting Information Fig. S45 was 35.0% in the group injected with mB4S combined with the anti-PD-L1 antibody, compared with 4.2% in the saline group, 10.7% in the EPI-treated group, 9.5% in the diABZI-treated group, 17.0% in the B4-treated group, 24.1% in the B4S-treated group, 8.7% in the anti-PD-L1 antibody-treated group, and 27.8% in the mB4S-treated group. The matured DCs in

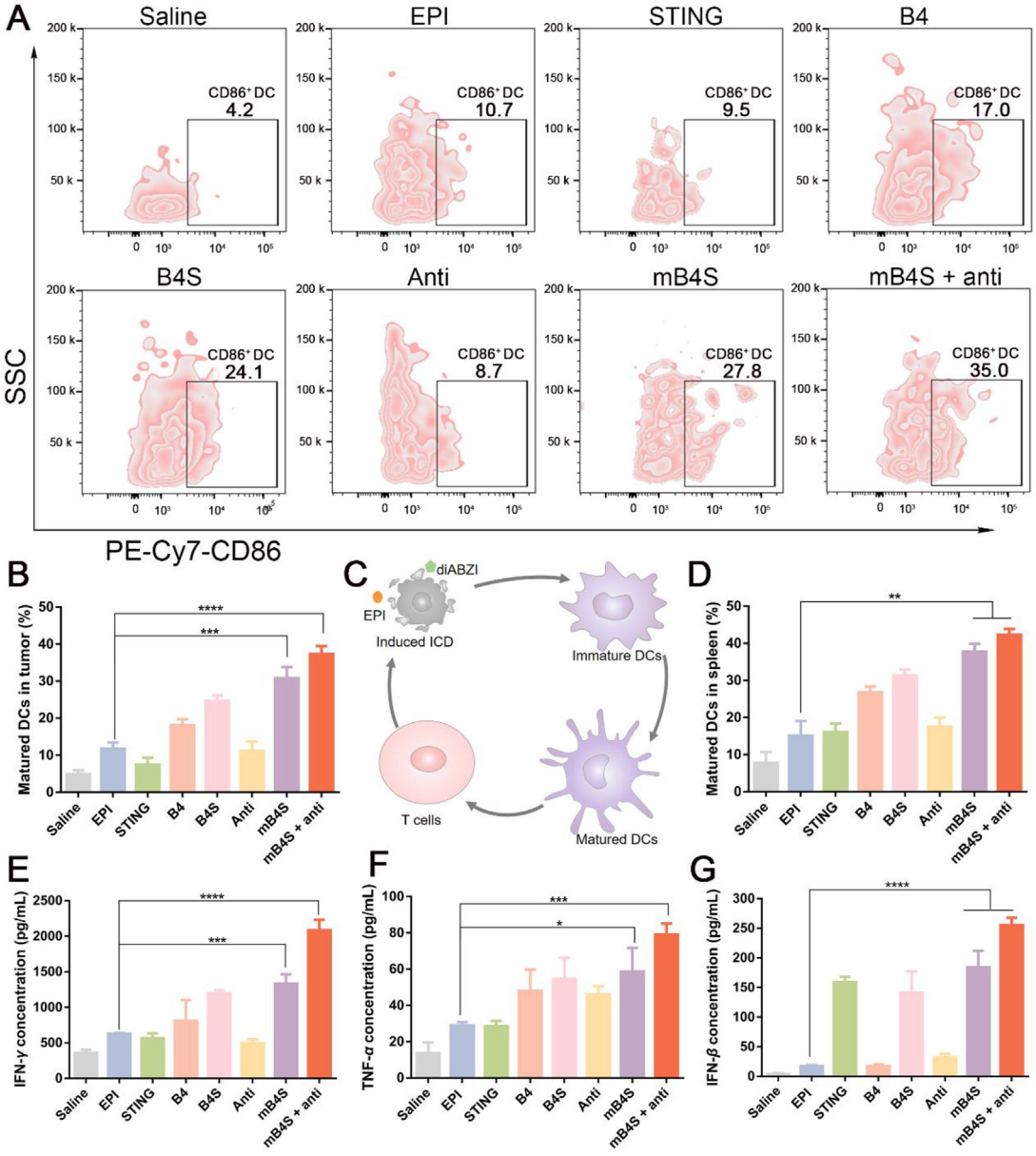

Figure 5 mB4S promoted DCs maturation and cytokines secretion. (A–B) Flow cytometry analysis of matured DCs ($CD11c^+MHC\ II^+CD86^+$) in the tumor tissue after treatment with saline, EPI, diABZI, B4, B4S, mB4S, anti-PD-L1 antibody, and mB4S + anti-PD-L1 antibody. (C) Schematic diagram for the mechanism of activating anti-tumor immune responses by EPI combined with diABZI. (D) The percentage of matured DCs in the spleen after different treatments. Cytokines including IFN-γ (E), TNF-α (F), and IFN-β (G) in the tumor tissue supernatant after the above treatments (Data are presented as mean ± SD, $n = 3$, $^*P < 0.05$, $^{**}P < 0.01$, $^{***}P < 0.001$ and $^{****}P < 0.0001$ *vs*. EPI-treated group).

the spleen were also analyzed and shown in Fig. 5D and Supporting Information Fig. S46. The frequency of matured DCs was raised to 39.2% in the group injected with mB4S, which was 2.19-fold of that in the EPI-injected group and 2.47-fold of that in the anti-PD-L1 antibody-injected group. These results strongly supported that EPI as an ICD inducer in combination with a STING agonist could significantly promote DCs maturation to initiate anti-tumor immune responses (Fig. 5C).

The majority of cytokines are small molecular functional peptides, and they are secreted by immune cells such as T lymphocytes, B lymphocytes, and NK cells[42]. As a messenger molecule of the immune system, cytokines build a bridge of communication between immune cells and help realize effective anti-tumor effects[43]. We collected the supernatant of the tumor tissues after different treatments for ELISA of the concentration of cytokines including IFN-γ, TNF-α, and IFN-β. As shown in Fig. 5E, the concentration

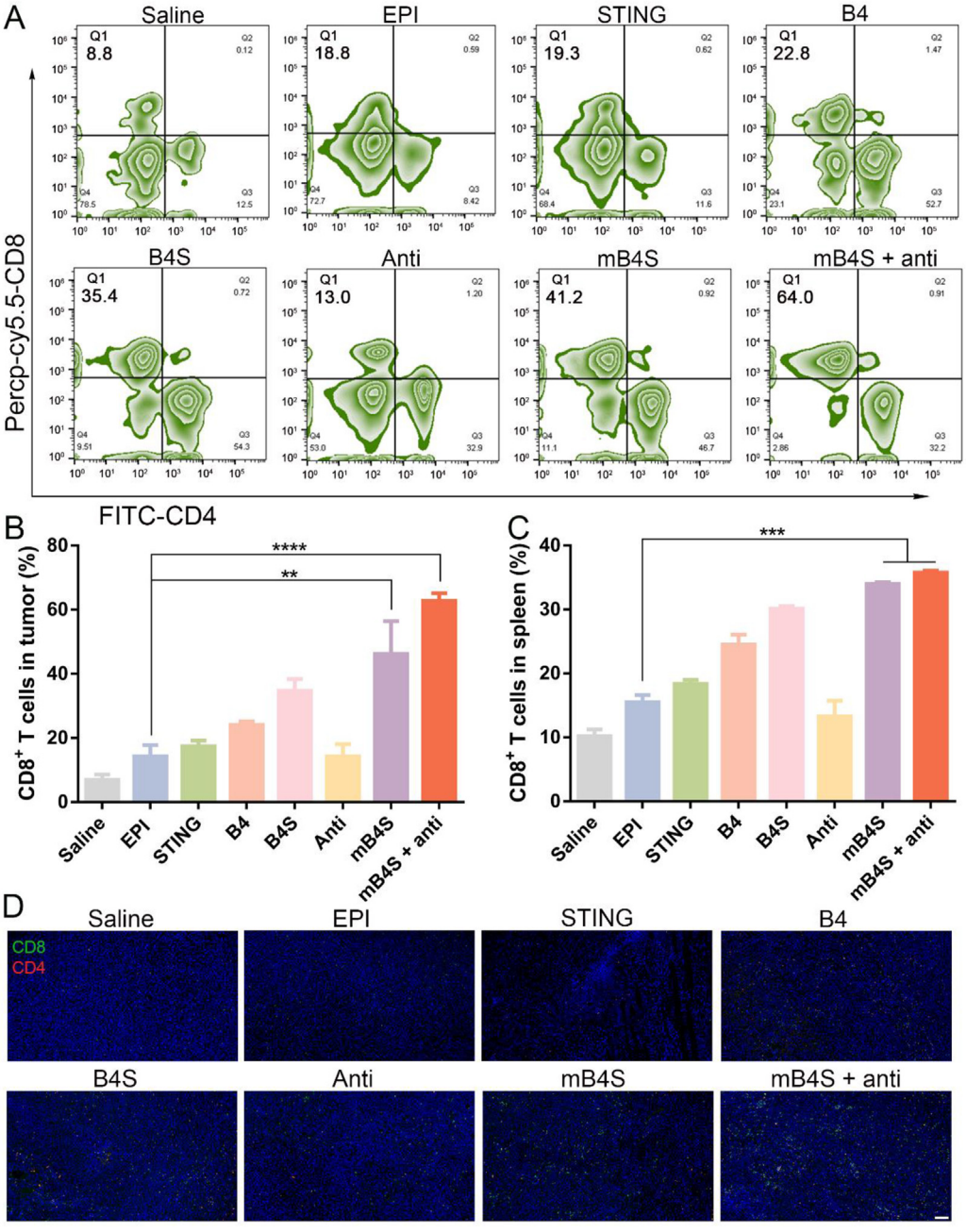

Figure 6 mB4S activated CD8$^+$ T cells for enhancing the anti-tumor immunity. (A) Representative flow cytometry plots of CD8$^+$ T cells (CD3$^+$CD8$^+$) in the tumor tissue after treatment with saline, EPI, diABZI, B4, B4S, B4S, mB4S, anti-PD-L1 antibody, and mB4S + anti-PD-L1 antibody. The percentage of CD8$^+$ T cells in the tumor tissue (B) and the spleen (C) in each treatment group was presented in histograms (Data are presented as mean ± SD, $n = 3$, $^{**}P < 0.01$, $^{***}P < 0.001$, $^{****}P < 0.0001$ *vs*. EPI-treated group). (D) Representative images of CD8$^+$ and CD4$^+$ T cells after immunofluorescent staining of the tumor tissue at the end of treatment (Blue: cell nuclei; Green: CD8$^+$ T cell; Red: CD4$^+$ T cells; scale bar = 100 μm).

of IFN-γ in the group treated with mB4S + anti-PD-L1 antibody was 2086.1 ± 147.7 pg/mL, while 632.8 ± 147.7 pg/mL in the EPI-treated group and 499.2 ± 53.5 pg/mL in the anti-PD-L1 antibody-treated group. The concentration of TNF-α in the group exposed to mB4S combined with the anti-PD-L1 antibody group was 1.72-fold of that in the anti-PD-L1 antibody-treated group (Fig. 5F). Furthermore, IFN-β secreted in the tumor tissue, an indicator for the activation of the STING pathway[44], displayed an incremental trend in the order of treatment by EPI, diABZI, mB4S, and mB4S plus the anti-PD-L1 antibody. The concentration in the mice group was 17.9 ± 2.1 pg/mL, 159.4 ± 8.7 pg/mL, 184.2 ± 3.1 pg/mL, and 255.3 ± 12.5 pg/mL (Fig. 5G), respectively, indicating that the combined therapy effectively activated the STING pathway to secrete IFN-β.

$CD8^+$ T cells are the key effector cells to kill tumor cells[45], and the proportion of $CD8^+$ T cells in the tumors is positively correlated with the efficacy of immunotherapy[46]. As shown in Fig. 6A and B with a gating strategy exhibited in Supporting Information Fig. S47, the percentage of $CD8^+$ T cells was 8.8%, 18.8%, 19.3%, 22.8%, 35.4%, and 41.2% after the treatment of saline, EPI, diABZI, B4, B4S, and mB4S, respectively, while it rose to 64.0% in the group treated with mB4S + anti-PD-L1 antibody, which was 4.92-fold of that in the anti-PD-L1 antibody-treated group (13.0%), indicating that the EPI prodrug-induced ICD in combination with the activated STING pathway effectively promoted infiltration of $CD8^+$ T cells into the tumor site. The immunofluorescent staining slices of the tumor tissues also supported that the treatment with mB4S in combination with the anti-PD-L1 antibody resulted in an increased frequency of $CD8^+$ T cells in the tumor tissue (Fig. 6D). In addition, the ratio of $CD8^+$ T cells was evaluated in the spleen (Fig. 6C and Supporting Information Fig. S48). It increased from 13.6% in the mice treated with the anti-PD-L1 antibody to 36.0% in the mice treated with mB4S + the antibody. These results indicated that mB4S effectively activated the STING pathway to promote cross-presentation of DCs and infiltration of $CD8^+$ T cells into the tumor tissue, which mediated anti-tumor immune responses.

The majority of myeloid-derived immune cells include TAMs and MDSCs, and they play an immunosuppressive role in the tumor

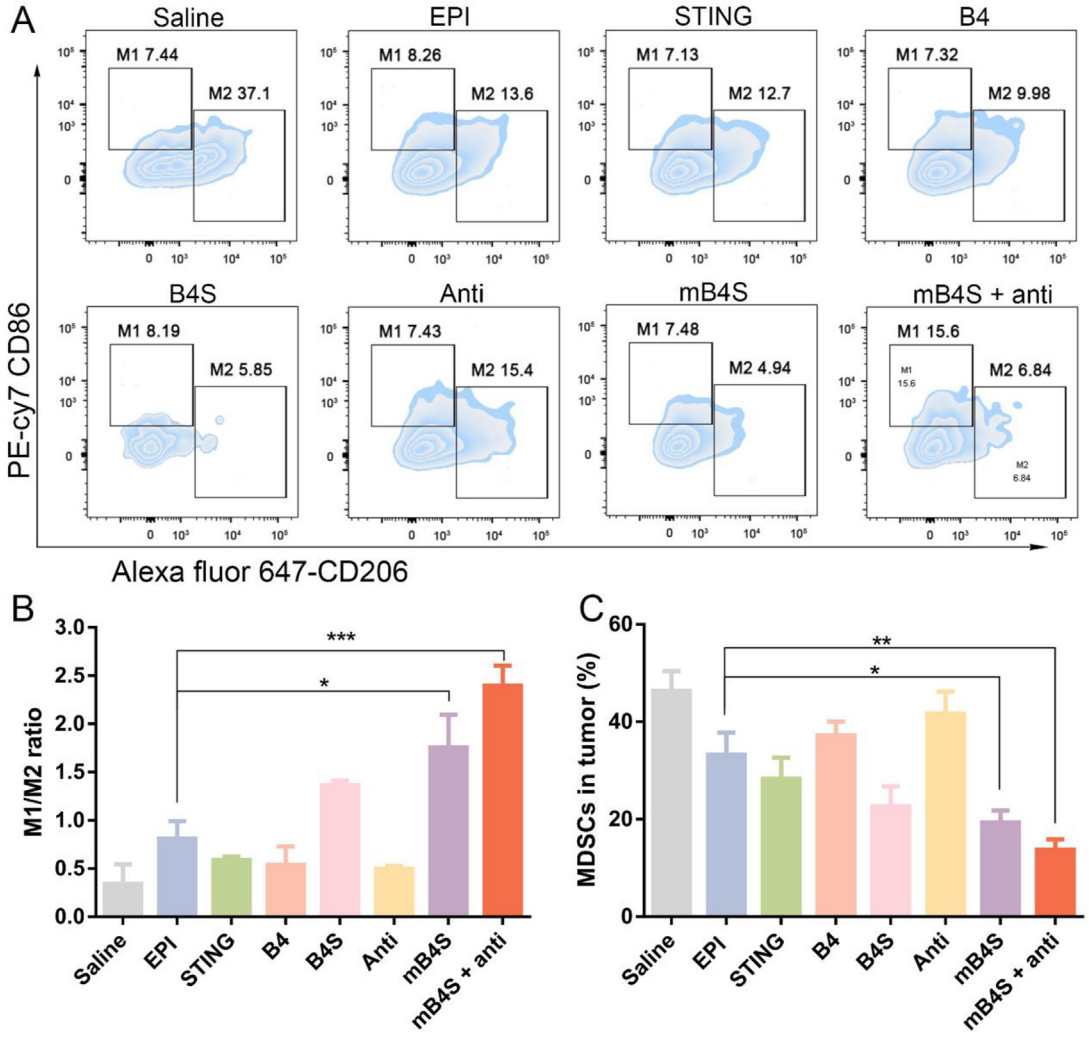

Figure 7 mB4S treatment up-regulated M1-like TAMs and down-regulated MDSCs in the tumor tissue. (A) Quantitation of M1-like TAMs ($CD11b^+F4/80^+CD86^+$) in the tumor tissue after different treatments *via* flow cytometry. (B) Statistic analysis of the ratio of the M1-like to the M2-like TAMs in the tumors. (C) The percentage of MDSCs ($CD11b^+Gr\text{-}1^+$) in the tumors of each treatment group (Data are presented as mean ± SD, $n = 3$, $^*P < 0.05$, $^{**}P < 0.01$, $^{***}P < 0.001$ *vs*. EPI treated group).

microenvironment[47]. The M1-like TAMs that are proinflammatory can phagocytose tumor cells, while the M2-like TAMs that are anti-inflammatory can promote tumor growth and invasion in the tumor tissue[48]. Activation of the STING pathway has been demonstrated to promote the production of M1-like TAMs and suppression of MDSCs in the tumor microenvironment[49,50]. The M1-like and M2-like TAMs were detected after different treatments *via* flow cytometry with a gating strategy exhibited in Supporting Information Fig. S49. As presented in Fig. 7A and B, the M1/M2 ratio in the tumors increased from 0.61 in the EPI-treated group to 1.51 in the mB4S-treated group, and 2.28 in the group treated with mB4S + anti-PD-L1 antibody. A significant increase in the M1/M2 ratio in the tumors suggested that this combined therapy of mB4S + anti-PD-L1 antibody could remarkably facilitate the production of the M1-like TAMs and reduce the M2-like TAMs. MDSCs can inhibit the normal innate and adaptive immune function of immune cells, and they play a negative regulatory role in the tumor microenvironment[51]. The percentage of MDSCs in the EPI-treated group was 38.2%, while it reduced to 21.1% in the mB4S-treated group and 14.8% in the mice treated with mB4S + anti-PD-L1 antibody (Fig. 7C and Supporting Information Fig. S50). These results suggest that mB4S-induced activation of the STING pathway could help remodel an immunosuppressive microenvironment to an immune-supportive one *via* up-regulation of the M1-like TAMs and down-regulation of MDSCs.

From the changes in the constitutional components of immune cells in the tumor microenvironment after different treatments, mB4S effectively induced ICD to promote the maturation of DCs for presentation of released tumor-associated antigens to T cells and the infiltration of $CD8^+$ T cells into the tumor microenvironment. Secretion of cytokines including IFN-γ, TNF-α, and IFN-β was significantly enhanced after the treatment of mB4S, leading to an improved ratio of M1-like to M2-like TAMs and down-regulation of immunosuppressive cells including MDSCs, which could create an immune-responsive microenvironment to boost the therapeutic effect of the anti-PD-L1 antibody in the 4T1-bearing mice.

4. Conclusions

In summary, we constructed cell membrane-coated polymeric prodrug nanoparticles containing EPI to induce ICD and diABZI to activate the STING pathway, which helped create an immune-responsive microenvironment to enhance the immunotherapeutic effect of anti-PD-L1 antibodies. Coating polymeric prodrug nanoparticles with the 4T1 cell membrane facilitated their cellular uptake by 4T1 cells. After internalization of cell membrane-coated polymeric prodrug nanoparticles, EPI was released to mediate apoptosis of tumor cells. CRT exposure was induced and ATP secretion enhanced in the 4T1 cells treated with mB4S to improve the tumor immunogenicity, and the STING agonist effectively activated the STING pathway *via* up-regulation of p-TBK1 and p-IFR-3. Importantly, the treatment with mB4S promoted DCs maturation and $CD8^+$ T cells infiltration into the tumor site, up-regulated the anti-tumor M1-like TAMs, and down-regulated immunosuppressive MDSCs, which could reverse the tumor immune environment from an immunosuppressive to immune-responsive one. Combined with an anti-PD-L1 antibody, mB4S displayed a potent anti-tumor effect in both 4T1-bearing mice and CT-26-bearing mice. This study suggests that a STING agonist combined with an ICD inducer could enhance tumor immunogenicity and facilitate $CD8^+$ T cells infiltration to create an immune-activated microenvironment for potentiating the anti-PD-L1 immunotherapeutic effect.

Acknowledgments

This work was supported by National Natural Science Foundation of China (32271445, 52073193, and 82202322), National Science and Technology Major Project of China (2023YFB3810004), 1·3·5 Project for Disciplines of Excellence, West China Hospital, Sichuan University (ZYJC21013, China), the Sichuan Science and Technology Program (2023NSFSC1592, China), the China Postdoctoral Science Foundation (2021M692255, China) and the Post-Doctor Research Project, West China Hospital, Sichuan University (2020HXBH094, China). Thanks to Guiping Yuan for her help of TEM images, and Zhiqian Li, Zhengju Chen, Yan Wang, Xiangyi Ren, Cong Li, Lei Wu and Yaping Wu (Histology and Imaging Platform, Research Core Facility, West China Hospital, Sichuan University) for their help in confocal imaging studies and Qiaorong Huang, Wentong Meng and Xue Li (Laboratory of Stem Cell Biology, West China Hospital, Sichuan University) for their help in flow cytometer.

Author contributions

Zhilin Li: Conceptualization, Methodology, Investigation, Data curation, Formal analysis, Visualization, Writing-original draft preparation. Qianfeng Zhang: Methodology, Investigation, Data curation, Formal analysis. Zhiqian Li: Methodology, Investigation. Long Ren: Methodology, Formal analysis. Danyi Pan: Methodology, Formal analysis. Qiyong Gong: Supervision, Project administration. Zhongwei Gu: Supervision, Project administration. Hao Cai: Methodology, Investigation, Data curation, Formal analysis, Writing-original draft preparation, Funding acquisition, Project administration. Kui Luo: Supervision, Funding acquisition, Project administration, Resources, Writing-review & editing.

Conflicts of interest

The authors declare no conflicts of interest.

Appendix A. Supplementary data

Supplementary data to this article can be found online at https://doi.org/10.1016/j.apsb.2024.02.006.

References

1. Ribas A, Wolchok JD. Cancer immunotherapy using checkpoint blockade. *Science* 2018;**359**:1350−5.
2. Topalian SL, Weiner GJ, Pardoll DM. Cancer immunotherapy comes of age. *J Clin Oncol* 2011;**29**:4828−36.
3. Keenan TE, Tolaney SM. Role of immunotherapy in triple-negative breast cancer. *J Natl Compr Cancer Netw* 2020;**18**:479−89.
4. Polk A, Svane IM, Andersson M, Nielsen D. Checkpoint inhibitors in breast cancer—current status. *Cancer Treat Rev* 2018;**63**:122−34.
5. Sharma P, Hu-Lieskovan S, Wargo JA, Ribas A. Primary, adaptive, and acquired resistance to cancer immunotherapy. *Cell* 2017;**168**:707−23.
6. Savas P, Loi S. Expanding the role for immunotherapy in triple-negative breast cancer. *Cancer Cell* 2020;**37**:623−4.
7. Savas P, Loi S. Metastatic breast cancer: TIL it is too late. *Clin Cancer Res* 2020;**26**:526−8.

8. Galon J, Bruni D. Approaches to treat immune hot, altered and cold tumours with combination immunotherapies. *Nat Rev Drug Discov* 2019;**18**:197−218.
9. Duan QQ, Zhang HL, Zheng JN, Zhang LJ. Turning cold into hot: firing up the tumor microenvironment. *Trends Cancer* 2020;**6**:605−18.
10. Xu YY, Xiong JY, Sun XY, Gao HL. Targeted nanomedicines remodeling immunosuppressive tumor microenvironment for enhanced cancer immunotherapy. *Acta Pharm Sin B* 2022;**12**: 4327−47.
11. Kroemer G, Galluzzi L, Kepp O, Zitvogel L. Immunogenic cell death in cancer therapy. *Annu Rev Immunol* 2013;**31**:51−72.
12. Li L, Li YC, Yang CH, Radford DC, Wang JW, Janát-Amsbury M, et al. Inhibition of immunosuppressive tumors by polymer-assisted inductions of immunogenic cell death and multivalent PD-L1 cross-linking. *Adv Funct Mater* 2020;**30**:1908961.
13. Pelras T, Loos K. Strategies for the synthesis of sequence-controlled glycopolymers and their potential for advanced applications. *Prog Polym Sci* 2021;**117**:101393.
14. Stenzel MH. Glycopolymers for drug delivery: opportunities and challenges. *Macromolecules* 2022;**55**:4867−90.
15. Zhu R, Jiang W, Pu YJ, Luo K, Wu Y, He B, et al. Functionalization of magnetic nanoparticles with peptide dendrimers. *J Mater Chem* 2011; **21**:5464−74.
16. Cook AB, Perrier S. Branched and dendritic polymer architectures: functional nanomaterials for therapeutic delivery. *Adv Funct Mater* 2020;**30**:1901001.
17. Luo K, Liu G, Zhang XW, She WC, He B, Nie Y, et al. Functional L-lysine dendritic macromolecules as liver-imaging probes. *Macromol Biosci* 2009;**9**:1227−36.
18. Li HN, Feng Y, Luo Q, Li ZQ, Li X, Gan HT, et al. Stimuli-activatable nanomedicine meets cancer theranostics. *Theranostics* 2023;**13**: 5386−417.
19. Cai H, Dai XH, Wang XJ, Tan P, Gu L, Luo Q, et al. A nanostrategy for efficient imaging-guided antitumor therapy through a stimuli-responsive branched polymeric prodrug. *Adv Sci* 2020;**7**:1903243.
20. Luo Q, Duan ZY, Li X, Gu L, Ren L, Zhu HY, et al. Branched polymer-based redox/enzyme-activatable photodynamic nanoagent to trigger STING-dependent immune responses for enhanced therapeutic effect. *Adv Funct Mater* 2022;**32**:2110408.
21. Gu L, Duan ZY, Li X, Li X, Li YG, Li XL, et al. Enzyme-triggered deep tumor penetration of a dual-drug nanomedicine enables an enhanced cancer combination therapy. *Bioact Mater* 2023;**26**: 102−15.
22. Fang RH, Gao WW, Zhang LF. Targeting drugs to tumours using cell membrane-coated nanoparticles. *Nat Rev Clin Oncol* 2023;**20**:33−48.
23. Li RX, He YW, Zhang SY, Qin J, Wang JX. Cell membrane-based nanoparticles: a new biomimetic platform for tumor diagnosis and treatment. *Acta Pharm Sin B* 2018;**8**:14−22.
24. Burdette DL, Monroe KM, Sotelo-Troha K, Iwig JS, Eckert B, Hyodo M, et al. STING is a direct innate immune sensor of cyclic di-GMP. *Nature* 2011;**478**:515−8.
25. Man SM, Jenkins BJ. Context-dependent functions of pattern recognition receptors in cancer. *Nat Rev Cancer* 2022;**22**:397−413.
26. Ding CY, Song ZL, Shen AC, Chen TT, Zhang A. Small molecules targeting the innate immune cGAS−STING−TBK1 signaling pathway. *Acta Pharm Sin B* 2020;**10**:2272−98.
27. Dunn GP, Bruce AT, Sheehan KC, Shankaran V, Uppaluri R, Bui JD, et al. A critical function for type I interferons in cancer immunoediting. *Nat Immunol* 2005;**6**:722−9.
28. Woo SR, Fuertes MB, Corrales L, Spranger S, Furdyna MJ, Leung MY, et al. STING-dependent cytosolic DNA sensing mediates innate immune recognition of immunogenic tumors. *Immunity* 2014; **41**:830−42.
29. Ramanjulu JM, Pesiridis GS, Yang JS, Concha N, Singhaus R, Zhang SY, et al. Design of amidobenzimidazole STING receptor agonists with systemic activity. *Nature* 2018;**564**:439−43.
30. Liu YJ, Lu X, Qin N, Qiao YT, Xing SS, Liu WY, et al. STING, a promising target for small molecular immune modulator: a review. *Eur J Med Chem* 2021;**211**:113113.
31. Kroll AV, Fang RH, Jiang Y, Zhou JR, Wei XL, Yu CL, et al. Nanoparticulate delivery of cancer cell membrane elicits multiantigenic antitumor immunity. *Adv Mater* 2017;**29**:1703969.
32. Koziolová E, Kostka L, Kotrchová L, Šubr V, Konefal R, Nottelet B, et al. *N*-(2-Hydroxypropyl)methacrylamide-based linear, diblock, and starlike polymer drug carriers: advanced process for their simple production. *Biomacromolecules* 2018;**19**:4003−13.
33. Chen Z, Zhao PF, Luo ZY, Zheng MB, Tian H, Gong P, et al. Cancer cell membrane-biomimetic nanoparticles for homologous-targeting dual-modal imaging and photothermal therapy. *ACS Nano* 2016;**10**:10049−57.
34. Van Herck S, Feng B, Tang L. Delivery of STING agonists for adjuvanting subunit vaccines. *Adv Drug Deliv Rev* 2021;**179**:114020.
35. Krysko DV, Garg AD, Kaczmarek A, Krysko O, Agostinis P, Vandenabeele P. Immunogenic cell death and DAMPs in cancer therapy. *Nat Rev Cancer* 2012;**12**:860−75.
36. Cun JE, Fan X, Pan PP, Gao WX, Luo K, He B, et al. Copper-based metal−organic frameworks for biomedical applications. *Adv Colloid Interfac* 2022;**305**:102686.
37. Glinsky VV, Glinsky GV, Glinskii OV, Huxley VH, Turk JR, Mossine VV, et al. Intravascular metastatic cancer cell homotypic aggregation at the sites of primary attachment to the endothelium. *Cancer Res* 2003;**63**:3805−11.
38. Ou Y, Chen K, Cai H, Zhang H, Gong QY, Wang J, et al. Enzyme/pH-sensitive polyHPMA−DOX conjugate as a biocompatible and efficient anticancer agent. *Biomater Sci* 2018;**6**:1177−88.
39. Li JH, Zhang XQ, Zhao MY, Wu LH, Luo K, Pu YJ, et al. Tumor-pH-sensitive PLLA-based microsphere with acid cleavable acetal bonds on the backbone for efficient localized chemotherapy. *Biomacromolecules* 2018;**19**:3140−8.
40. Jenkins RW, Barbie DA, Flaherty KT. Mechanisms of resistance to immune checkpoint inhibitors. *Br J Cancer* 2018;**118**:9−16.
41. Chen DS, Mellman I. Oncology meets immunology: the cancer-immunity cycle. *Immunity* 2013;**39**:1−10.
42. O'Shea JJ, Murray PJ. Cytokine signaling modules in inflammatory responses. *Immunity* 2008;**28**:477−87.
43. Propper DJ, Balkwill FR. Harnessing cytokines and chemokines for cancer therapy. *Nat Rev Clin Oncol* 2022;**19**:237−53.
44. Fuertes MB, Woo SR, Burnett B, Fu YX, Gajewski TF. Type I interferon response and innate immune sensing of cancer. *Trends Immunol* 2013;**34**:67−73.
45. Philip M, Schietinger A. $CD8^+$ T cell differentiation and dysfunction in cancer. *Nat Rev Immunol* 2022;**22**:209−23.
46. Wang QD, Qin Y, Li B. $CD8^+$ T cell exhaustion and cancer immunotherapy. *Cancer Lett* 2023;**559**:216043.
47. Gabrilovich DI, Ostrand-Rosenberg S, Bronte V. Coordinated regulation of myeloid cells by tumours. *Nat Rev Immunol* 2012;**12**:253−68.
48. DeNardo DG, Ruffell B. Macrophages as regulators of tumour immunity and immunotherapy. *Nat Rev Immunol* 2019;**19**:369−82.
49. Wu YT, Fang Y, Wei Q, Shi HP, Tan HL, Deng YF, et al. Tumor-targeted delivery of a STING agonist improvescancer immunotherapy. *Proc Natl Acad Sci U S A* 2022;**119**:e2214278119.
50. Kho VM, Mekers VE, Span PN, Bussink J, Adema GJ. Radiotherapy and cGAS/STING signaling: impact on MDSCs in the tumor microenvironment. *Cell Immunol* 2021;**362**:104298.
51. Mandula JK, Rodriguez PC. Tumor-directed dysregulation of erythroid progenitors drives immunosuppressive myeloid cells. *Cancer Cell* 2022;**40**:597−9.